# Contents

# Chapter 1

# QD Solar Cells

This chapter gives a brief overview over the fundamental principles of photovoltaic cells and QD solar cells in particular, then focusing on the example of PbS cells to give some specific information.

## 1.1 Solar Cell Principles

The basic idea of a solar cell is to convert light into electrical power. Light is absorbed in a material, thus generating an electron-hole pair. The generated electrons and holes must then be separted and conducted to electrodes attached to the material. The accumulation of carriers at the eletrodes generates a potential difference, and a current will flow between the electrodes if a load is connected.
The carrier separation can be achieved by an electirc field inside the material. Different types of solar cells exist based on different approaches. The classical silicon solar cell uses a semiconductor p-n junction: When a photon (with energy greater than the bandgap) is absorbed in the semiconductor, an electron is promoted from the valence to the conduction band. Near the junction, these photogenerated electrons and holes are swept away to different sides due to the built-in electric field of the p-n junction (fig. **??**).
Other approaches are also widely used, for example shottky-contacts (metal-semiconductor interface) or semiconductor-liquid interfaces.

The electrical behaviour of a photovoltaic cell can be well described by its I-V characteristics (fig. **??**). In the dark, the cell behaves like a diode (in the case of a p-n junction solar cell this seems fairly obvious). Under illumination, the curve is shifted vertically downwards. It crosses now the fourth quadrant, where the electrical power $P = IV$ is negative, which indicates that power is delivered to the load.

To characterise the solar cell, there are some common parameters, which are mentioned in the following paragraph. The open-circuit voltage $V_{OC}$, which is the maximum voltage provided by the cell, and directly related to the energy band structure and thus built-in potential. The short-circuit current $I_{SC}$, giving the maximum current if the electrodes are connected. $I_{SC}$ is proportional to the carrier density under illumination and to the carrier mobility, which are therefore important parameters to maximise.
An often used quantity is the *fill factor (FF)*, which gives the ratio between the maximum power $P_M = I_M V_M$ and the product $I_{SC}V_{OC}$. It describes how well behaved the I-V characteristics is (the more the curve approaches a rechtangular shape, the better).
Of practical importance for comparing solar cells is the power conversion efficiency $\eta$, giving the ratio of optical power which is converted into electrical power.

$$\eta = \frac{P_{max}}{P_{in}} = FF\frac{I_{SC}V_{OC}}{P_{in}}$$

Usually an optical source called AM1.5 is used, whose spectral intensity distribution matches that of sunlight reaching the eart's surface at an angle of 48.2°. [3]

## 1.2 Solar Cells using cQDs

Semiconductor nano crystal solids, can be used for solar cells. Thus nano crystals (NC) made of CdSe, CdTe, PbSe, PbS and many more can be used for this purpose. Like with bulk semiconductors, heterojunction solar cells are possible (using materials with different band gaps), such as CdSe-CdTe cells [3]. Similarly, using Schottky-contacs is also an option.

Using NC solids made of QDs offers several advantages. One big advantage is the possibilty of choosing the size of the band gap by controlling the size of the QDs, which can be done easily during the synthesis of CQDs. Controlling the band gap means essentially choosing the spectrum which can be absorbed, and consequently cells which can make use of a broad spectrum can be engineered.
Furthermore QD solar cells are easy to fabricate and that at low costs. Large-scale production would also be possible [3].
Using NC solids, there are promising perspectives for more advanced techniques, in order to increase efficiency. These invlove e.g. carrier multiplication (the absorption of one highly energetic photon causes the creation multiple electron-hole pairs) or hot carrier solar cells (electrons in higher energy states in the conduction band are extracted before they relax to the band edge and lose some energy).

However, there are some problems which have to be overcome. One is the (air-) stability and lifespan of QD based photovoltaic cells. In many cases, the devices lose dramatically in efficiency after some time, which can be as short as hours or even minutes [7]. Another problem is the currently rather low efficiency of the cells (maxium acchieved efficiency of around 7% for a PbS cell [5]). One issue leading to reduced efficiency is the presence of undesired states in the band gap (mid-gap or trap states). These arise due to 'dangling' (unbound) bonds of surface atoms, and are significant in a QD, since its surface to volume ratio is high. So-called *passivation* of the surface is thus very important.
Furthermore, for furture large-scale production, the materials used in the production process should be cheap, plentiful available and preferably non-toxic, which contrasts with some NC materials that contain toxic elements like Cd or Pb.

### 1.2.1 Example of a PbS QD Solar Cell

Since the structure and fabrication methods of QD solar cell are quite diverse, we will focus here on a PbS QD solar cell, as they were produced at ETH at the Laboratory for Nanoelectronics [6]. Due to the small band gap of PbS (0.37eV for bulk PbS), the solar cell is able to convert power from the near infrared spectrum. This is of interest since roughly 50% of the solar energy that reaches the earth is in the infrared spectrum.

#### Structure

The principle part of the cell is a Schottky junction of PbS and Al, with a thin protection layer (1 nm) of LiF in between. The Schottky barrier is responsible for the electric field which separates the photogenerated carriers. The Al Cathode is covered by a layer of silver, for better air stability. The transparent anode is formed of a layer of indium tin oxide (ITO), on top of the PbS (fig. **??**).

#### Fabrication Process

The main steps involved in the fabrication are described below, as they were carried out in reference [6].
We start with a glass substrate, which is coated with ITO by lithography. The sample has then to be cleaned (using solvents, and afterwards by $O_2$ plasma treatment to remove organic residuals).
In the next step, the active layer, i.e. the PbS QDs, is deposited. This can be done by dip coating, where the substrate is immersed in a PbS-hexane solution, and taken out after a few seconds, leaving a thin film of the solution on the sample. Alternatively, spin coating can be used, where several drops of the PbS-Hexane solution are dropped on the substrate, which is then rotated to spread the drops, leading to a film of homogeneous thickness.
Now the long ligands surrounding the QDs have to be exchanged for short ligands, in order to improve inter-particle coupling (and thus e.g. carrier mobility). For this purpose, the substrate is immersed into a suitable compound: Ethandithiol, benzenedithiol (both organic), and ammonium thiocyanate ($NH_4SCN$, inorganic) can be used.
The sample is then rinsed in acetonitrile and or hexane. In order to obtain a PbS film of desired thickness, the steps of spin (respectively dip) coating, ligand exchange and rinsing have to be repeated several times.
In a last step, the cathode, i.e. the three layers of LiF, Al and Ag are evaporated on the substrate.

# Chapter 2

# Analysis of PbS QD simulation data

In this chapter we will take a look at the simulation data. We will try to make an analysis of the energy levels and wavefunction of PbS QDs and draw some conclusions.

There are a few practical aspects to note concerning the simulation of PbS QDs with OMEN : Since OMEN will consider in its calculation 20 orbitals for the PbS atoms, one must keep in mind that the simulation uses significantly more computing resources than a simulation of, for instance, a CdSe-CdS QD. Especially the memory usage during the calculation can easily exceed 10GB for larger QDs. The size of the generated simulation data for one QD can also amount to more than 100MB. Another problem is the high degeneracy of energylevels close to the bandedge. This makes it necessarry to simulate a higher number of modes, thus increasing the usage of resources further.

## 2.1 Energy leves

Remark: In the following discussion, the terms conduction band, band edge and so on are used. Although there are, no energy bands present in a QD, but rather discrete energy levels, these terms nevertheless make some sense, since the states above the 'band gap' are similar to conduction band states, and those below to valence band states, respectively. 'Conduction band' thus refers in this context to the discrete energy states above the band gap.
Taking a look at the eigenenergies close to the bandedge, one can see that there are 8 closely spaced modes, for conduction and valence band respectively. Generally, closest to the bandedge there is a twofold degenerate energy level, followed by a fourfold degenerate level and then again a twofold degenerate level. (For a few simulations the order is different, for example the fourfold degenerate energy level is closest to the band edge.)
As the size of the QDs increases, the energy levels get closer to each other, resulting in higher degeneracy. This is shown in figure 2.1 (a), (b), (d), where the energy levels (including degeneracy) are shown for 2, 6 and 10nm QDs. Since some levels are very closely spaced, they are not clearly distinguishable form each

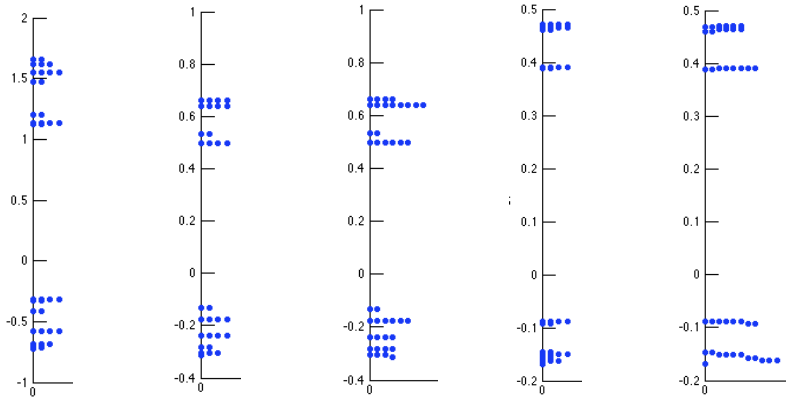


Figure 2.1: Energy levels for different sized QDs: 2nm (a), 6nm (b) and (c), 10nm (d) and (e). Vertical axis in eV. Multiple dots on the horizontal axis signify degeneracy. In plots (c) and (e) energies within 0.03eV are plottet as degenerate, for better visibility.

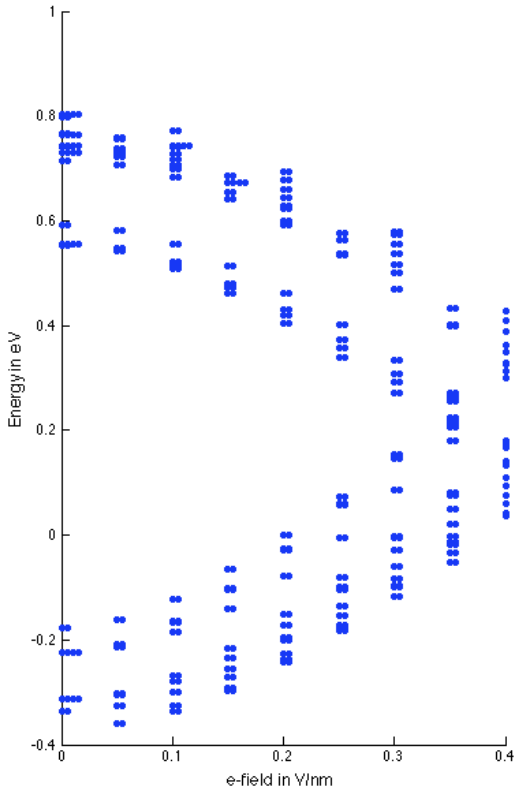


Figure 2.2: Energy states (including degeneracy) for different electric fields.

other. For this reason, the tolerance, within wich an energy level is shown as degenerate, was increased to 0.03 in figure 2.1 (c), (e). An effective eightfold degeneracy for the 10nm QD is now clearly visible.

In the presence of an electric field, this degeneracy is broken, leading to more energy levels, which are all, interestingly, twofold degenerate. This is shown in figure 2.2 for a 5nm QD, where the energy levels are plotted against applied electric field. One can also clearly see how the bandgap gets smaller, as is discussed later on.

### 2.1.1 Bandgap

### 2.1.2 Bandgap of QDs in presence of an electric field

## 2.2 Wave functions

### 2.2.1 Modes and shape of the wave functions

#### QDs bigger than 3nm

Sometimes, the wave functions of QDs are described in analogy to atomic orbitals, labeling them S, P, D and so on, with subscript e or h, denoting electron-like (conduction band) states or hole-like (valence band) states respectively. We will see how well this picture corresponds to the simulation.

The 8 energy states ('modes') closest to the band edge (for conduction and valence band respectively) have wave functions with spherical symmetry, where the highest probability density in the center (fig. 2.3). This is in agreement with the 8 predicted $1S_{e,h}$ orbitals for PbS [3].

The higher energy states show wave functions with more complex shapes. For example, a 8nm QD shows the following wave function shapes: After the 8 spherical conduction band states follow 4 (degenerate) states with barbell shape, in different orientations. Then 2 states with spherical shell shape. After that, 2 states with a shape similar to two crossed barbells. Then again 2 spherical shell-like states, followed by 2 ring-shaped wave functions, and so on (fig. 2.4). For the valence band states, the shapes are similar, although they do not occur in the same order (the same is true for QDs of different sizes). This is however not consistent with the expected 24 1P orbitals, TODO

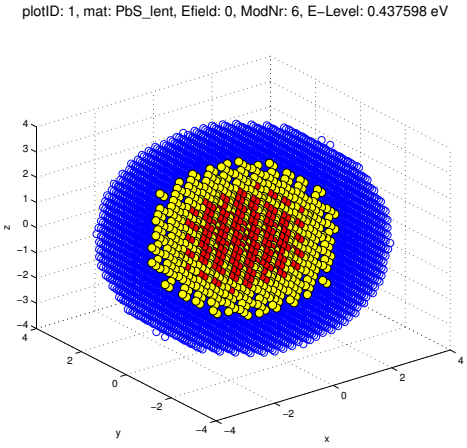


Figure 2.3: Probability density for an energy state in the lower conduction band of an 8nm QD. Locations of very high probability are shown in red, those of medium to high probability in yellow.

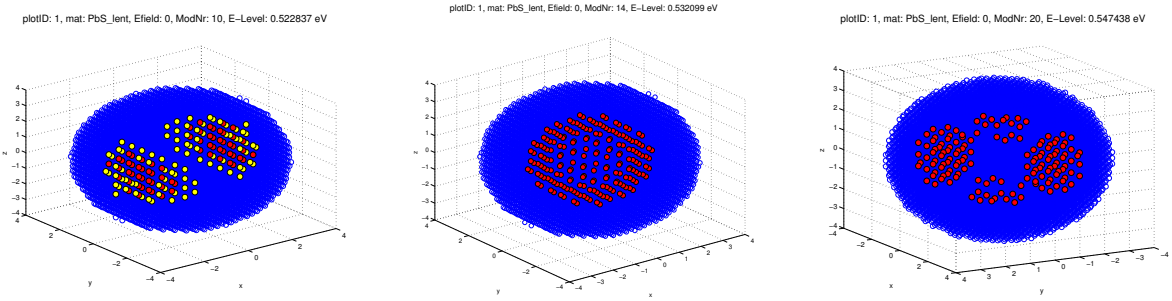


(a) (b) (c)

Figure 2.4: Probability density for higher energy states in an 8nm QD: barbell-shape (a), spherical shell-shape (b), crossed barbell-shape (c). In plots (b) and (c) the locations of medium high probability (yellow points) are not shown for clarity.

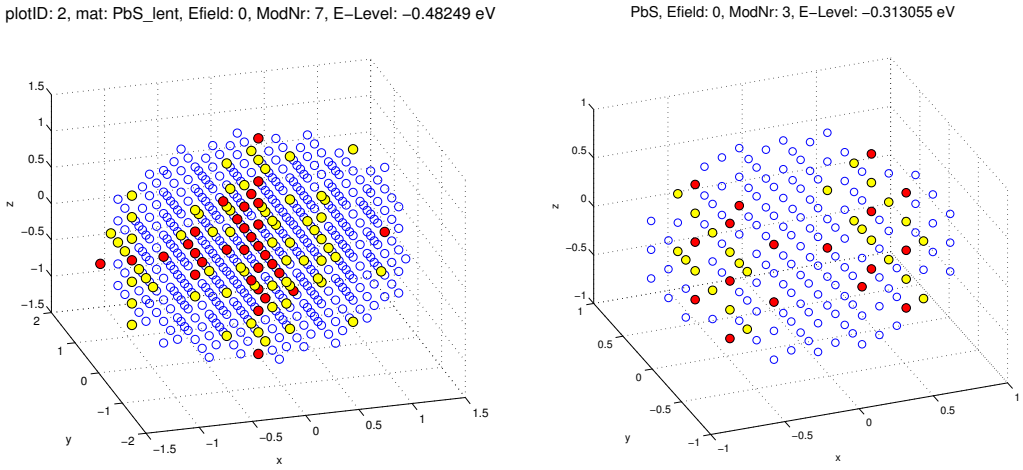


(a) 3nm QD. 7th valence band state. (b) 2nm QD. 3rd valence band state.

Figure 2.5: Probability density for valence band states. The shape starts to deviate from the previously spherical shapes.

**QDs smaller than 3nm**

For QDs smaller than 3nm, the problem is that it is more difficult to see the shape of the wavefunction (too few atoms). Furthermore it is not clear how well this models a real QD, since the surface (and thus passivation of the surface) beginns to have an even bigger influence.
For a 2 and 3nm QDs, the 8 lowest conduction band states still remain more or less spherical. Whereas the valence band states start loose spherical symetry. For a 3nm QD, mode 7 and 8 are already slightly asymetric (fig. 2.5 (a)), and for the 2nm QD even modes 1 to 4 are clearly not spherical, but the wave function is rather localised at two sides (fig. 2.5 (b)).

### 2.2.2 Influence of an electirc field

The presence of an electric field results in a shift of the wave function, i.e. the maximum of the probability density is not in the center anymore and the spherical symetry of the 8 first states is broken (for conduction and valence band respectively). Furthermore, one can see that the valence band states really behave differently than conduction band states: The wave function is shifted in the opposite direction (fig. 2.6). This confirms that the valence band states are hole-like, similar to semiconductor band theory.
For larger electric fields the bandgap gets smaller until it finally disappears, i.e. conduction and valence band states are not separated anymore. For example, for a 5nm QD, the band gap disappers for electirc fields larger than 0.35 V/nm (fig. 2.2). The states which are close to the (former) band gap cannot be sepearted in conduction and valence band: as energy increases, some hole-like states (below 0.313 eV) are followed by electron-like (i.e. conduction band-like) states (0.325 ... 0.329 eV) which then again are followed by hole-like states (around 0.348 eV) and later again electron-like states (fig. 2.7).
Additionally, with higher electric fields, the wave functions seem not only to be shifted, but change shape: Some now look more like asymetric barbells or even stranger, ring-like shapes (fig. 2.7 (a) and (f)).

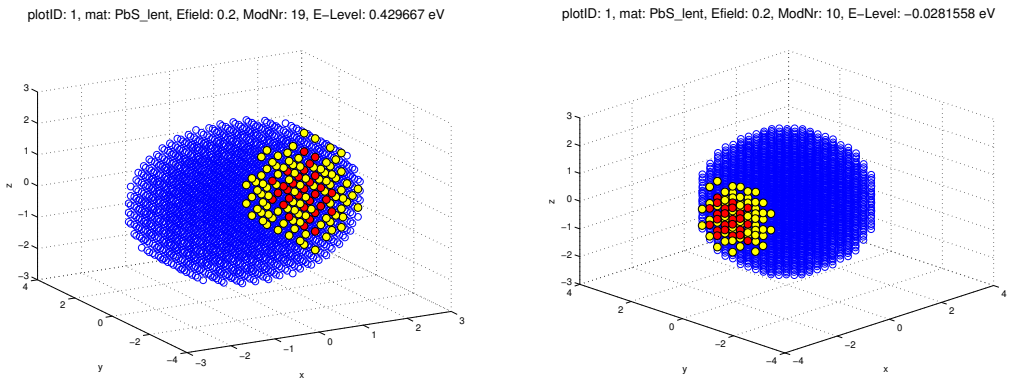


(a) conduction band state (b) valence band state

Figure 2.6: Probability densities for a 5nm QD in an electic field of 0.2V/nm.

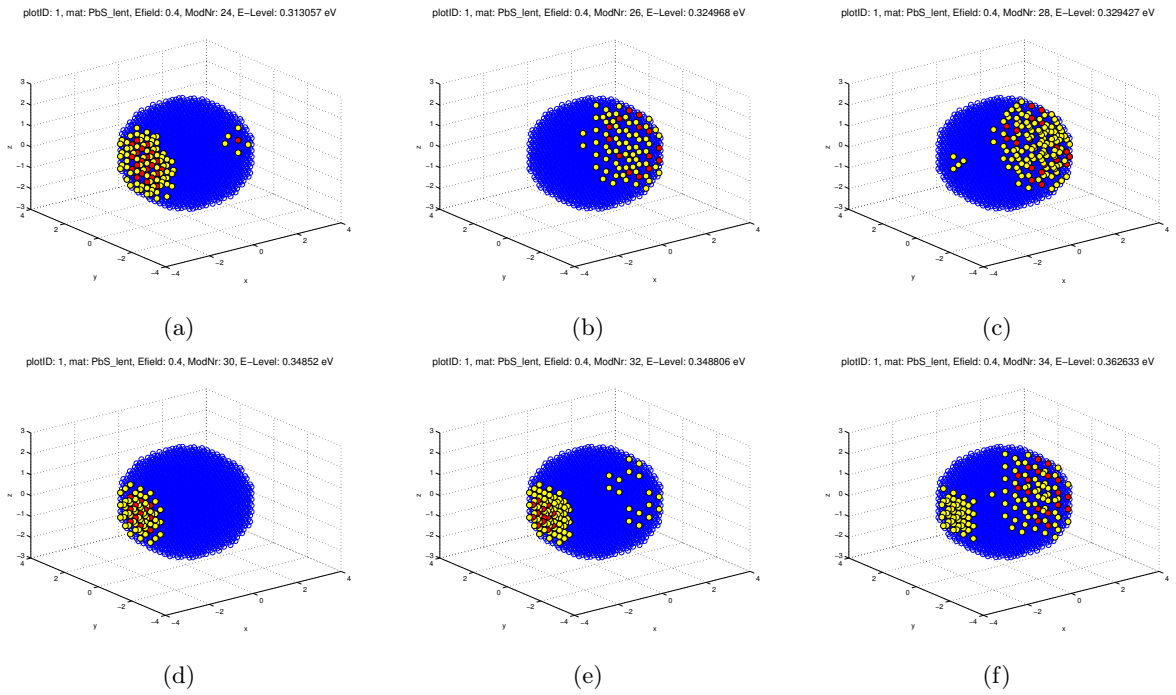


Figure 2.7: Probability density in the presence of a high electric field (0.4V/nm). Increasing energy from (a) to (f). Hole-like states (a, d, e) become mixed with electron-like states (b, c, f).

## 2.3 conclusions

Some bla

# Bibliography


[1] John D. Dow Robert S. Allgaier Otto F. Sankey Craig S. Lent, Marshall A. Bowen and Eliza S. Ho. Relativistic empirical tight-binding theory of the energy bands of gete, snte, pbte, pbse, pbs, and their alloys. *Superlattices and Microstructures*, 2(5):491–499, 1986.

[2] Olesya Yarema Deniz Bozyigit, Michael Jakob and Vanessa Wood. Deep level transient spectroscopy (dlts) on colloidal-synthesized nanocrystal solids. November 2012.

[3] Maksym V. Kovalenko Dmitri V. Talapin, Jong-Soo Lee and Elena V. Shevchenko. Prospects of colloidal nanocrystals for electronic and optoelectronic applications. *Chemical Reviews*, 110(1):389–485, January 2010.

[4] Al. L. Efros and M. Rosen. The electronic structure of semiconductor nanocrystals. *Annual Review of Materials Science*, 30:475–521, 2000.

[5] Alexander H. Ip et. al. Hybrid passivated colloidal quantum dot solids. *nature nanotechnology*, 7(9):577–582, September 2012.

[6] Michael Jakob. Deep level transient spectroscopy on solar cells based on colloidal nanocrystals. September 2012.

[7] Edward H. Sargent Jiang Tang. Infrared colloidal quantum dots for photovoltaics: Fundamental and recent progress. *Advanced Materials*, 23(1):12–29, January 2011.

[8] Victor I. Klimov. *Nanocrystal Quantum Dots*. CRC Press, Second Edition edition, 2010.

[9] Gianluca Calestani Andrea Migliori Antonietta Guagliardi Ludovico Cademartiri, Erica Montanari and Geoffrey A. Ozin. Size-dependent extinction coefficients of pbs quantum dots. *Journal of the American Chemical Society*, 128(31):10337–10346, August 2006.

[10] Mathieu Luisier. *OMEN Manual*. ETH Zürich, Integrated Systems Laboratory, October 2012.

[11] Gregory D. Scholes Margaret A. Hines. Colloidal pbs nanocrystals with size-turnable near-infrared emission: Observation of post-synthesis self-narrowing of the particle size distribution. *Advanced Materials*, 15(21):1844–1849, November 2003.

# List of Tables